

IMPROVING SINGLE PARTICLE LOCALIZATION WITH AN EMPIRICALLY CALIBRATED GAUSSIAN KERNEL

Marcio de Moraes Marim, Bo Zhang, Jean-Christophe Olivo-Marin and Christophe Zimmer

Quantitative Image Analysis Group, Institut Pasteur, 25-28 rue du Docteur Roux, 75015 Paris

ABSTRACT

Accurate computational localization of single fluorescent particles is of interest to many biophysical studies and underlies recent approaches to high resolution microscopy using photo-switchable fluorophores. The position of individual particles is typically computed by least-squares fitting of a gaussian intensity profile to the image, whose band-width is either derived from an idealized theoretical model of the point spread function (PSF), or itself fitted to the image. However, the band-width best approximating the actual PSF may differ significantly from its theoretical value, while fitting it is expected to degrade localization accuracy. Here, instead, we measure the real PSF bandwidth using fluorescent beads as calibration probes, and use this new bandwidth in a Gaussian model fitting algorithm. We show on simulated and real images that this simple modification of the standard localization procedure results in significant improvement of the 3D accuracy in the nanometer range.

Index Terms — Fluorescence microscopy, localization accuracy, point spread function, super-resolution.

1. INTRODUCTION

A large number of cell biological problems can benefit from accurate estimations of the position of particles observed by static or dynamic microscopy. For example, localization and tracking of fluorescently labeled membrane proteins can inform about the biophysical properties and organization of the membrane, such as the presence of “rafts”. Similarly, tracking of chromatic loci allows to characterize its diffusion coefficients and/or the sizes of confining domains. In conventional fluorescence microscopy, the image of a point source is a blurred intensity distribution whose effective size (full width at half maximum) exceeds $200nm$ laterally and 2-3 times more along the microscope axis. Nevertheless, it is well known that the position of isolated particles can be determined with an accuracy that is not limited by the size of the PSF, but rather by the signal to noise ratio of the image [1]. In practice, accuracies of a few nanometers or less have been reported even for single molecules [2]. However, assemblies of numerous molecules within a diffraction limited spot could not be resolved. Recently, though, several groups have introduced super-

resolution microscopy techniques in which dense ensembles of photo-switchable molecules are activated and imaged sequentially such that only sparse subsets of molecules are fluorescent at any given time [3-5]. These optically isolated molecules can then be localized with high accuracy much as single particles. After repeating a large number of activation, imaging and localization cycles, the positions of all molecules in the focal plane are assembled into a single image, whose resolution is dictated only by the localization accuracy of the individual molecules and is currently estimated to $\sim 30 nm$ [4].

Both for single molecules studies and for super-resolution microscopy, molecules should be localized as accurately as possible. Typically, localization is performed by least-squares fitting of a 2D or 3D Gaussian kernel to the image [6, 7]. In this case, the bandwidth of the Gaussian kernel is either fitted to the object to be localized, which makes insufficient use of prior information, or is derived from theoretical approximations of an ideal diffraction-limited PSF [7, 8]. However such approximations do not account for aberrations due to imperfect alignment of the optics, mismatch of refractive index, etc. In practice, these sources of aberrations can induce substantial distortions from the theoretical PSF, as will be illustrated below. As a consequence, localization algorithms based on the theoretical values are expected to suffer from suboptimal performance. Here, we show that a very simple modification of the PSF model based on empirical data allows a non-negligible improvement in the localization accuracy.

2. METHODS

2.1 Empirical vs. theoretical gaussian PSF approximation

In a recent study, it was shown that an anisotropic gaussian kernel g with different lateral and axial bandwidths σ_{xy} and σ_z can provide a good approximation to the theoretical point spread function of a confocal or spinning disc microscope operating in the absence of any optical aberration [8].

$$g(x,y,z,\sigma_{xy},\sigma_z) = \exp\left(-\frac{(x-x_c)^2 + (y-y_c)^2}{2\sigma_{xy}^2} - \frac{(z-z_c)^2}{2\sigma_z^2}\right) \quad (1)$$

Under these assumptions, the axial and lateral bandwidths (σ_{xy}^{theo} , σ_z^{theo}) have been derived that provide the best fit to the theoretical PSF in the least-squares sense [8]. To measure the distortion due to optical aberrations not accounted for by this model, we imaged fluorescent beads of diameter $100nm$ dried on a coverslip. These beads can be considered with very high accuracy as point light sources. Fig. 1 compares a bead image obtained by a spinning disc microscope to the gaussian kernel (σ_{xy}^{theo} , σ_z^{theo}) = (77.7, 229.5) nm computed following [8] and using the following microscope parameters: excitation and emission wavelengths $\lambda_{ex}=0.488\mu m$ and $\lambda_{em}=0.5\mu m$, numerical aperture $NA=1.4$, refractive index $n=1.51$, pinhole size $d=1$ Airy unit = $0.44\mu m$. It is apparent from Fig.1, that the PSF is significantly distorted from its ideal theoretical shape due to optical aberrations.

2.2 Calibration of the gaussian kernel using bead images

The theoretical PSF approximation could in principle be extended to physically model the effect of different types of aberrations. Here, however, we chose a much simpler and pragmatic approach, consisting in approximating the PSF with a simple geometric model without identifying the cause of the aberrations. To do this, we retain the cylindrically symmetric gaussian kernel, but fitted the parameters (σ_{xy} , σ_z) to images of isolated beads used as calibration objects. This was done by a least-squares fit using an iterative non-linear optimization routine:

$$[A, \lambda_B, x_c, y_c, z_c, \sigma_{xy}, \sigma_z] = \operatorname{argmin} \left\{ \sum_{k=1}^M [Ag(x_k, y_k, z_k, \sigma_{xy}, \sigma_z) - I(x_k, y_k, z_k)]^2 \right\} \quad (2)$$

where A denotes the intensity of the bead, (x_c, y_c, z_c) are the coordinates of the bead center, $I(x, y, z)$ is the image grey-level at location (x, y, z) , M is the number of voxels and k is an index into the voxel. To obtain reliable statistics despite image noise, this fitting was repeated on >100 beads from several 3D image stacks.

The fitting procedure requires an initial guess of the bead position. To obtain it, we used a detection method based on a local spottiness score [7, 9] with a high threshold that keeps only the brightest beads. Despite this conservative detection scheme, the fitting may occasionally result in large values of σ_{xy} or σ_z caused by the close proximity of two beads or failure of the optimization (drastic spatial variations of the optical aberrations are unphysical).

After elimination of such outliers, we found mean values of the kernel bandwidth of $\langle \sigma_{xy}^{emp} \rangle = 123 \text{ nm}$ and $\langle \sigma_z^{emp} \rangle = 376 \text{ nm}$. Both values are approximately 60% larger than their theoretical counterparts, confirming that optical aberrations strongly distort the PSF width. The standard deviations of σ_{xy}^{emp} and σ_z^{emp} are only 3.4 nm and 15.6 nm , respectively, i.e. 2.7% and 4% of $\langle \sigma_{xy}^{emp} \rangle$ and

$\langle \sigma_z^{emp} \rangle$. The aberrated bandwidths are thus remarkably constant over the field of view. Furthermore, Fig. 1 illustrates that the aberrated kernel provides a good match to the real PSF. This justifies the use of a new kernel with the above parameters as a more realistic PSF model.

2.3 Improved localization method

Particle localization algorithms based on gaussian fits typically use either theoretical aberration-ignoring bandwidths [3, 7, 9] or estimate the bandwidth together with the position coordinates by fitting (as we have done in section 2.2 above). The latter approach is suboptimal for localizing sub-diffraction particles, since it does not use prior information on the PSF, and will therefore give poorer localization performance. Here, instead, we propose to localize particles by estimating the position and intensity parameters while keeping the kernel bandwidth fixed to the values (σ_{xy}^{emp} , σ_z^{emp}) previously estimated on bead images as just described:

$$[A, \lambda_B, x_c, y_c, z_c] = \operatorname{argmin} \left\{ \sum_{k=1}^M [Ag(x_k, y_k, z_k, \sigma_{xy}^{emp}, \sigma_z^{emp}) - I(x_k, y_k, z_k)]^2 \right\} \quad (3)$$

We will show in the following that this simple modification allows a significant improvement of the localization accuracy.

2.4 Simulation of test images

To validate our method, we created synthetic images of subresolution objects blurred by a Gaussian kernel with $\sigma_{xy} = 123nm$ and $\sigma_z^{emp} = 376nm$ and corrupted by a mixture of Poisson and Gaussian noise:

$$I = \alpha \cdot \text{Poisson} \left(\sum_{k=1}^M Ag(x_k, y_k, z_k) + \lambda_B \right) + N(\mu, \sigma^2) \quad (4)$$

where α is the effective gain of the system, λ_B is the mean intensity of the background and N is a normal distribution with mean intensity μ and standard deviation σ . The SNR of the images can then be computed from:

$$SNR = \frac{\alpha A}{\sqrt{\alpha^2(A + \lambda_B) + \sigma^2}} \quad (5)$$

To generate simulations matching the noise characteristics of the real bead images, we measured these parameters on images of both beads and background. The mixed-Poisson-Gaussian noise parameters (α , λ_B , μ , σ) are estimated using cumulant matching method [10], and we obtained $\alpha=101.2$, $\lambda_B=0.42$, $\mu=1076.1$, $\sigma=42$, $A=12$ for the real image yielding an $SNR=2.7$.

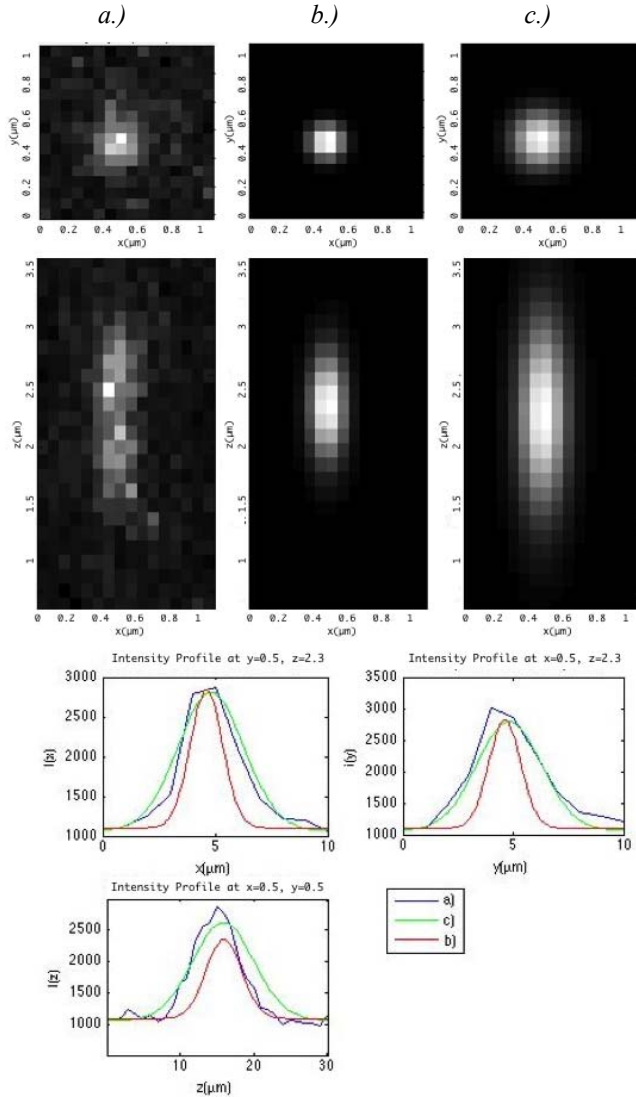


Fig.1. Real vs. theoretical PSF. The top and bottom rows show maximum intensity projections of 3D stacks along z and y , respectively. (a) real image of a bead with diameter of 100 nanometer; (b) theoretical Gaussian with $\sigma_{xy}^{theo}=77.7\text{ nm}$ and $\sigma_z^{theo}=229.5\text{ nm}$; (c) empirical Gaussian with $\sigma_{xy}^{emp}=123\text{ nm}$ and $\sigma_z^{emp}=376\text{ nm}$. The bottom curves show intensity profiles across the three images along the three axis (x,y,z).

3. EXPERIMENTAL RESULTS

3.1. Measuring localization accuracy

To evaluate the performance of the new kernel in localization, we use both simulated and real images. Localization accuracy is usually measured by the standard deviation of the error in position estimates. This quantity

can be immediately computed for simulated data as $s_x = std(x_i - x_{i,0})$, where $x_{i,0}$ is the real coordinate of the bead i , std denotes standard deviation over all N beads $i=1..N$ and x_i is the estimated coordinate; s_y and s_z are defined similarly.

For real images, a ground truth is not directly accessible. However as we are using beads labeled with two fluorophores of wavelengths $\lambda_{em1}=0.5\mu\text{m}$ (green) and $\lambda_{em2}=0.6\mu\text{m}$ (red), the difference in positions of the same bead estimated from two independent color channels can be used as an indirect measure of localization accuracy. Assuming that localization errors in the two color channels G and R are independent of each other and identically distributed, we estimate the localization accuracy along direction x (and similarly for y and z) by:

$$s_x' = \frac{std(x_i^G - x_i^R)}{\sqrt{2}} \quad (6)$$

where x_i^G and x_i^R are the x -coordinates estimated in the two color channels and i designates a bead detected in both color channels (beads detected in one color channel without detection in the other channel in close vicinity are discarded).

3.2. Results

We evaluated the localization accuracy both on simulated (see section 2.4) and real bead images. Results are summarized in Table 1. First, we verify on the simulated data that localization accuracy improves for higher SNR ratios [1], with perfect localization for noise-free images (within numerical errors). Second, localization results on real bead images confirm that accuracies in the range of $\sim 10\text{ nm}$ and less can be achieved. Third, this accuracy is improved by 25-35% using the empirically calibrated rather than the theoretical Gaussian. This is a significant improvement and shows that more realistic PSF approximations are useful for accurate particle localization.

Could accuracy be more significantly improved using more complex PSF models than the simple Gaussian kernel employed here? To address this, we simulated images with a perfectly Gaussian PSF with $\sigma_{xy}^{emp} = 123\text{ nm}$ and $\sigma_z^{emp} = 376\text{ nm}$ and noise parameters matched to the real image. For these simulated images, the accuracy is only $\sim 20\text{-}35\%$ better than for the real bead images when localization is done with the empirically calibrated Gaussian. This means that our Gaussian kernel captures most of the optical aberrations that affect localization, and that more complicated approximations to the real PSF will yield at best a smaller additional improvement in accuracy. Thus, by adopting the empirically calibrated Gaussian kernel proposed here, the accuracy remains essentially limited only by the SNR or the limitations of the algorithms rather than the PSF model.

	number of beads	SNR	localization accuracy (nm)		
			x	y	z
beads	197	2.71	4.3 (5.4)	4.6 (6.6)	15.0 (21.5)
simulated	100	$+\infty$	$\sim 10^{-7}$	$\sim 10^{-7}$	$\sim 10^{-7}$
images of beads	100	10	0.8 (1.0)	0.9 (1.0)	2.1 (2.2)
	100	4.4	2.0 (2.6)	2.1 (2.6)	7.1 (8.3)
	100	2.7	3.5 (4.2)	3.4 (4.8)	11.7 (12.3)

Table.1. Localization accuracy with theoretical (brackets) and empirically calibrated (bold) Gaussian PSF approximation. Accuracy is defined as explained in section 3.1, and SNR as in section 2.4.

4. CONCLUSION

We have shown that the localization accuracy of least-squares Gaussian fitting algorithms can be improved simply by calibrating the bandwidth on real images of fluorescent probes. In our examples on spinning disc microscopes, we have obtained an improvement of accuracy of $\sim 30\%$, but larger improvements are expected if aberrations are more pronounced, as for example in wide-field microscopy.

Extensions of this study should replace the widely used least-squares fitting by the maximum likelihood estimator adapted to the presence of Poisson noise [1], which should further improve accuracy. It would also be of interest to use fluorescent beads embedded at varying heights in a 3D volume rather than lying on coverlips to study the depth-dependence of optical aberrations. We plan to address these issues in future work.

5. ACKNOWLEDGEMENTS

We thank Christophe Machu of the Imaging Platform and Axel Berger for acquiring the bead images. This work was funded by Institut Pasteur.

5. REFERENCES

[1] Ober, R.J., Ram, S., and Ward, E.S.: "Localization accuracy in single-molecule microscopy", *Biophys J*, 86, (2), pp. 1185-1200, 2004.

[2] Yildiz, A., Forkey, J.N., McKinney, S.A., Ha, T., Goldman, Y.E., and Selvin, P.R.: "Myosin V walks hand-over-hand: single fluorophore imaging with 1.5-nm localization", *Science*, 300, (5628), pp. 2061-2065, 2003.

[3] Betzig, E., Patterson, G.H., Sougrat, R., Lindwasser, O.W., Olenych, S., Bonifacino, J.S., Davidson, M.W., Lippincott-Schwartz, J., and Hess, H.F.: "Imaging intracellular fluorescent proteins at nanometer resolution", *Science*, 313, (5793), pp. 1642-1645, 2006.

[4] Bates, M., Huang, B., Dempsey, G.T., and Zhuang, X.: "Multicolor Super-Resolution Imaging with Photo-Switchable Fluorescent Probes", *Science*, pp. 1146598v1146591, 2007.

[5] Hess, S.T., Girirajan, T.P., and Mason, M.D.: "Ultra-high resolution imaging by fluorescence photoactivation localization microscopy", *Biophys J*, 91, (11), pp. 4258-4272, 2006.

[6] Cheezum, M.K., Walker, W.F., and Guilford, W.H.: "Quantitative comparison of algorithms for tracking single fluorescent particles", *Biophys J*, 81, (4), pp. 2378-2388, 2001.

[7] Thomann, D., Rines, D.R., Sorger, P.K., and Danuser, G.: "Automatic fluorescent tag detection in 3D with super-resolution: application to the analysis of chromosome movement", *J Microsc*, 208, (Pt 1), pp. 49-64, 2002.

[8] Zhang, B., Zerubia, J., and Olivo-Marin, J.C.: "Gaussian approximations of fluorescence microscope point-spread function models", *Appl Opt*, 46, (10), pp. 1819-1829, 2007.

[9] B. Zhang, J. M. Fadili, and J.-L. Starck, "Multi-scale variance stabilizing transform for multi-dimensional Poisson count image denoising", *IEEE International Conference on Acoustics, Speech and Signal Processing*, vol. 2, pp. 81-84, 2006.